Energy spectra in turbulent bubbly flows

Vivek N. Prakash[1,2], **J. Martínez Mercado**[1], **Leen van Wijngaarden**[1],
E. Mancilla[1,3], **Y. Tagawa**[1,4], **Detlef Lohse**[1,5] **and Chao Sun**[1,6,†]

[1]Physics of Fluids Group, Faculty of Science and Technology, J.M. Burgers Center for Fluid Dynamics, University of Twente, P.O. Box 217, 7500 AE Enschede, The Netherlands

[2]Department of Bioengineering, Stanford University, Stanford, CA 94305, USA

[3]Instituto de Investigaciones en Materiales, Universidad Nacional Autónoma de México, México Distrito Federal 04510, México

[4]Department of Mechanical Systems Engineering, Tokyo University of Agriculture and Technology, 1848588, Koganei-city, Tokyo, Japan

[5]Max Planck Institute for Dynamics and Self-Organization, D-37077 Göttingen, Germany

[6]Center for Combustion Energy and Department of Thermal Engineering, Tsinghua University, Beijing 100084, China

We conduct experiments in a turbulent bubbly flow to study the nature of the transition between the classical $-5/3$ energy spectrum scaling for a single-phase turbulent flow and the -3 scaling for a swarm of bubbles rising in a quiescent liquid and of bubble-dominated turbulence. The bubblance parameter (Lance & Bataille *J. Fluid Mech.*, vol. 222, 1991, pp. 95–118; Rensen *et al.*, *J. Fluid Mech.*, vol. 538, 2005, pp. 153–187), which measures the ratio of the bubble-induced kinetic energy to the kinetic energy induced by the turbulent liquid fluctuations before bubble injection, is often used to characterise bubbly flow. We vary the bubblance parameter from $b = \infty$ (pseudoturbulence) to $b = 0$ (single-phase flow) over 2–3 orders of magnitude (0.01–5) to study its effect on the turbulent energy spectrum and fluctuations in liquid velocity. The probability density functions (PDFs) of the fluctuations in liquid velocity show deviations from the Gaussian profile for $b > 0$, i.e. when bubbles are present in the system. The PDFs are asymmetric with higher probability in the positive tails. The energy spectra are found to follow the -3 scaling at length scales smaller than the size of the bubbles for bubbly flows. This -3 spectrum scaling holds not only in the well-established case of pseudoturbulence, but surprisingly in all cases where bubbles are present in the system ($b > 0$). Therefore, it is a generic feature of turbulent bubbly flows, and the bubblance parameter is probably not a suitable parameter to characterise the energy spectrum in bubbly turbulent flows. The physical reason is that the energy input by the bubbles passes over only to higher wavenumbers, and the energy production due to the bubbles can be directly balanced by the viscous dissipation in the bubble wakes as suggested by Lance & Bataille (1991). In addition, we provide an alternative explanation by balancing the energy production of the bubbles with viscous dissipation in the Fourier space.

Key words: gas/liquid flow, multiphase and particle-laden flows, turbulent flows

---

† Email address for correspondence: chaosun@tsinghua.edu.cn

1. Introduction

Turbulent bubbly flow has important industrial applications such as in chemical industries and steel plants (Deckwer 1992). A fundamental understanding of the influence of bubbles on turbulence is crucial for better designs and optimal utilisation of resources (Magnaudet & Eames 2000, Ern *et al.* 2012). In this work, we investigate the effect of bubbles on properties such as velocity fluctuations and energy spectra of turbulent flows. In turbulent bubbly flows the energy input in the liquid comes both from the bubbles and from external forcing. Depending on this source of energy input we can distinguish different regimes. Various parameters have been used to characterise these regimes. One of these is the 'bubblance' b (Lance & Bataille 1991, Rensen, Luther & Lohse 2005), defined as

$$b = \frac{1}{2} \frac{\alpha U_r^2}{u_0'^2}, \qquad (1.1)$$

where α is the bubble concentration (void fraction), U_r is the bubble rise velocity in still water and u_0' is the typical turbulent liquid fluctuation in the absence of bubbles.

We see that the case $b = 0$ represents single-phase turbulence (Pope 2000) and $b = \infty$ the situation where the fluctuating velocities are purely caused by bubbles. The latter regime is often called pseudoturbulence, and has been extensively investigated experimentally. A few early studies (e.g. Mudde, Groen & van der Akker 1997; Cui & Fan 2004) reported a Kolmogorov type of spectral density behaviour, a dependence on the wavenumber k as $k^{-5/3}$. However, recent work (Martinez Mercado *et al.* 2010; Mendez-Diaz *et al.* 2013; Riboux, Legendre & Risso 2013) clearly established that the spectral density in pseudoturbulence behaves as k^{-3}. In fact, the -3 spectrum scaling is found to be robust even if the bubble size is changed, or if liquids of higher viscosity are used instead of water. The recent study by Mendez-Diaz *et al.* (2013) suggests that the specific details of the hydrodynamic interactions among bubbles do not influence the way in which the pseudoturbulent fluctuations are produced. The current understanding is that the bubble-induced turbulence mainly results from the bubble wakes. The importance of the bubble wakes to the -3 spectrum scaling has also been established using numerical simulations by comparing the spectrum scalings between point-like bubble simulations (Mazzitelli & Lohse 2009) and fully resolved simulations of freely rising deformable bubbles (Roghair *et al.* 2011), with the former giving $-5/3$ due to the absence of wakes, and the latter fully resolved simulations giving -3 as the spectral scaling exponent.

Previous work has mainly been concerned with the extreme values of the b parameter, i.e. either pseudoturbulence ($b = \infty$) or single-phase turbulence ($b = 0$). Our focus in this paper is to study what happens in between these extremes because the energy spectrum scaling and the statistics of fluctuation in liquid velocity are not well known for large ranges of intermediate b. In this paper, we thus want to systematically analyse the flow as a function of the b parameter between the cases of single-phase turbulence ($b = 0$) and turbulence with some bubbles ($0 < b < 5$). The b parameter is varied over 2–3 orders of magnitude, namely from 0.01 to 5, and the pseudoturbulent case $b = \infty$ is also included. Pioneering experiments in turbulent bubbly flow were made by Lance & Bataille (1991) using hot-wire and laser Doppler anemometry (LDA). Their experiments did not cover a broad range of b. They found that with increasing α the Kolmogorov $k^{-5/3}$ spectral density is progressively substituted by a $k^{-8/3}$ behaviour. Lance & Bataille (1991) attributed this to the wakes of the bubbles. Here eddies are produced that are so rapidly dissipated
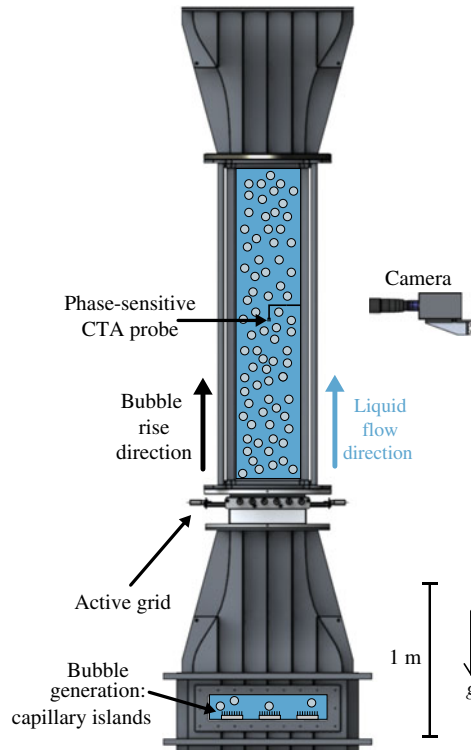
FIGURE 1. (Colour online) The Twente Water Tunnel (TWT) facility: a vertical multiphase water tunnel where homogeneous and isotropic turbulence is generated by an active grid. Air is blown through capillary islands located below the measurement section to generate bubbles. The bubbles rise and the liquid also flows in the upward direction, and the phase-sensitive CTA probe measures the fluctuations in liquid velocity.

that they do not take part in the energy cascade. Omitting then the transport term in the energy balance in k space, they concluded a k^{-3} behaviour on dimensional grounds. Referring to the definition of b in (1.1), one would expect a different spectral scaling depending on the energy input. For $b \ll 1$, the turbulent fluctuations would be dominant and the spectrum exponent would consequently be close to $-5/3$. When $b \gg 1$, bubble-induced fluctuations would dominate and the exponent would be close to -3. In the present work the parameter b is varied by adding external turbulence of varying intensity, which is produced using an active grid.

In the next section, we describe the experimental set-up, tools and methods used. This is followed by the results section, where we describe our findings for the fluctuations in liquid velocity and energy spectra. We provide an interpretation of our results in the discussion section, where we also summarise our work.

2. Experiments

2.1. *Experimental set-up*

The experiments are carried out in the Twente Water Tunnel (TWT) facility, which is an 8 m high vertical water tunnel (see figure 1). The measurement section of the TWT (dimensions: 2 m × 0.45 m × 0.45 m) is made of transparent glass to provide optical

Set 1 (3–5 mm bubbles)				Set 2 (2–4 mm bubbles)			
b	α (%)	u'_0 (cm s^{-1})	U_l (cm s^{-1})	b	α (%)	u'_0 (cm s^{-1})	U_l (cm s^{-1})
∞	2	0	0	∞	2	0	0
∞	1.17	0	0	∞	1.5	0	0
4.13	1	0.8	10	∞	1	0	0
2.06	0.5	0.8	10	∞	0.8	0	0
1.03	1	1.6	20	∞	0.5	0	0
0.78	0.75	1.6	20	4.13	1	0.8	10
0.52	0.5	1.6	20	2.06	0.5	0.8	10
0.17	0.67	3.2	40	1.03	1	1.6	20
0.08	0.3	3.2	40	0.78	0.75	1.6	20
0.03	0.17	4	50	0.52	0.5	1.6	20
0.01	0.083	4.8	60	0.37	0.8	2.4	30
0	0	2.4	30	0.23	0.5	2.4	30
				0.21	0.2	1.6	20
				0.15	0.6	3.2	40
				0.08	0.3	3.2	40
				0.03	0.2	4	50
				0	0	2.4	30

TABLE 1. Experimental parameters, set 1: 3–5 mm bubbles generated using capillary needles of inner diameter 500 µm, set 2: 2–4 mm bubbles produced using capillary needles of inner diameter 120 µm.

access for flow visualisation and measurements. We place the phase-sensitive constant-temperature anemometry (CTA) (hot-film) probe in the centre of this measurement section; more details of this technique are discussed in the next section. An active grid is used to generate nearly homogeneous and isotropic turbulent flow in the liquid phase and it is placed below the test section (Poorte & Biesheuvel 2002; Martinez Mercado *et al.* 2012; Prakash *et al.* 2012). Air bubbles are generated by blowing air through islands of capillary needles that are located below the measurement section. A U-tube set-up mounted in the measurement section is used to measure the gas void fraction α (see Rensen *et al.* 2005; Martinez Mercado *et al.* 2010 for more details). The bubbles pass through the active grid, rise through the measurement section and eventually escape through an open vent at the top of the TWT. The liquid flow is driven by a pump that recirculates the water throughout the TWT. The bubbles rise along with the upward mean flow in the measurement section; the system is thus a coflowing turbulent upward bubbly flow.

In our experiments, we vary the bubble diameter by changing the inner diameter of the capillary needles in the bubble-generating islands. Two different needles are used in our experiments: air bubbles of diameter 3–5 mm are generated using capillary needles of inner diameter 500 µm, and 2–4 mm bubbles are produced using the needles with inner diameter 120 µm. We classify our experiments into two sets based on the bubble diameter: experiments with bubbles of diameter 3–5 mm belong to set 1, and experiments with bubbles of diameter 2–4 mm are referred to as set 2 (see table 1). The purpose of exploring different bubble diameters in sets 1 and 2 is to test for size effects and to achieve a wider range of b values.

In the present experiments, the b parameter is varied by changing: (i) the volume flow rate of air through the capillary islands (i.e. equivalent to changing the gas void

fraction α), and (ii) the magnitude of the mean flow speed of water in the upward direction (to effectively change the turbulence intensity u'_0). In (1.1), U_r is the typical rise velocity of bubbles (in still water). We assume the value of the rise velocity of bubbles in still water, $U_r \approx 23$ cm s^{-1}, which is reasonable because it holds for the range of bubble diameters for both datasets (2–5 mm) considered in this study (see figure 7.3 in Clift, Grace & Weber (1978)).

We obtain b parameter values from ∞ to 0 by varying the void fraction (from 2 % to 0 %) and the mean flow velocity (0–60 cm s^{-1}). Table 1 lists all the different parameters varied in the present experiments. The turbulent flow properties (e.g. u'_0) are characterised by combined CTA–LDA measurements of only the liquid phase at different mean flow speeds (for details see Martinez Mercado *et al.* (2012)). The Kolmogorov scales range from 410 to 200 μm for mean flow speeds ranging between 20 and 60 cm s^{-1} respectively. For the same range of mean flow speeds, the Taylor length scales range between 10 and 6 mm, and the integral length scales are about 60 mm.

2.2. *High-speed imaging*

In order to visualise the flow, a Photron-PCI 1024 high-speed camera was focused on a vertical plane at the centre of the measurement section. We acquired two-dimensional images of each experiment using the camera (at 1000 Hz) and some of these snapshots are shown in figure 2. The $b = \infty$ experiments are shown in figure 2(*a,b*) where the gas void fractions are $\alpha = 2$ % and 1 %, respectively. The dense nature of the flow at such void fractions is evident: the flow is opaque and the phase-sensitive CTA probe is barely visible. As we proceed to look at the other cases in figure 2(*c–f*), α decreases, and the liquid mean flow speeds (U_l) increase, corresponding to a decrease in the b parameter from ∞ to 0.03. In our experiments, the bubbles must pass through the active grid, which consists of randomly oscillating steel flaps (a few rotations per second) to generate the required turbulence. At any given instant in time, the active grid is 50 % transparent (open) to the flow. Hence, the bubbles face a slight obstruction and sometimes interact with the steel flaps. The bubble–flap interaction, however, causes fragmentation of the bubbles and results in a decrease in the diameter of the bubbles. This decrease in bubble diameter becomes apparent at higher liquid mean flow speeds (U_l), as seen in figure 2(*c–f*). In our experiments, the CTA probe is placed sufficiently far away ($\approx$1 m) from the source of turbulence (active grid) so that the large-scale eddy motions and other transients have decayed and the turbulence is almost homogeneous and isotropic at the location of the probe. The probe is located at a distance where the fluctuation in downstream root-mean-square streamwise velocity does not vary significantly (see Poorte & Biesheuvel (2002) for a comparison between the present active grid and the more traditional passive grids).

We obtain a quantitative measurement of the bubble diameter using the images acquired (figure 2) from the individual experiments. The bubbles deform greatly over time, and given the dense nature (high α) of the flows, there is currently no reliable automated image processing algorithm available to accurately determine the bubble diameter. Hence, we had to resort to a manual procedure – where individual bubble boundaries are marked using mouse clicks in the open-source software ImageJ. An ellipse is fitted to the deformed bubble boundaries, and the equivalent bubble diameter is calculated as $d_b = \sqrt[3]{d_l^2 d_s}$, where d_l and d_s are the long and short axes of the ellipsoidal bubble. In each experiment, we measure the diameters of $\approx$50–100
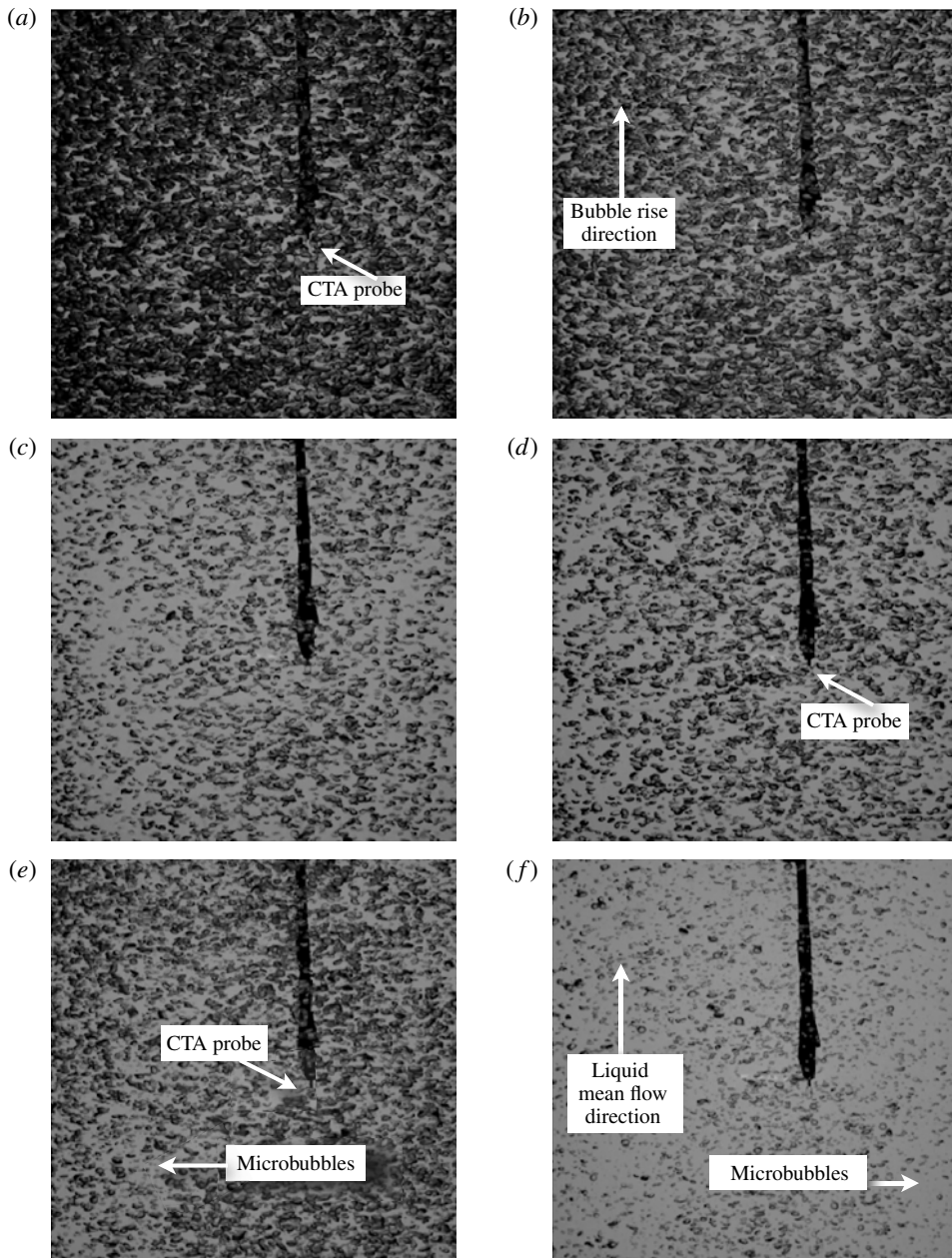
FIGURE 2. Snapshots from the experiments (set 1, see table 1) in different conditions.
(*a*) $b = \infty$, $U_l = 0$, $\alpha = 2\,\%$, (*b*) $b = \infty$, $U_l = 0$, $\alpha = 1\,\%$, (*c*) $b = 2.4$, $U_l = 10$ cm s^{-1},
$\alpha = 0.5\,\%$, (*d*) $b = 0.6$, $U_l = 20$ cm s^{-1}, $\alpha = 0.5\,\%$, (*e*) $b = 0.2$, $U_l = 40$ cm s^{-1}, $\alpha = 0.67\,\%$,
(*f*) $b = 0.03$, $U_l = 50$ cm s^{-1}, $\alpha = 0.17\,\%$.

bubble samples, and then take the mean value of the distribution to be the equivalent
diameter of the bubble. In figure 3 we observe that the bubble diameter decreases
with decreasing b parameter (increasing liquid mean flow speeds). The decrease
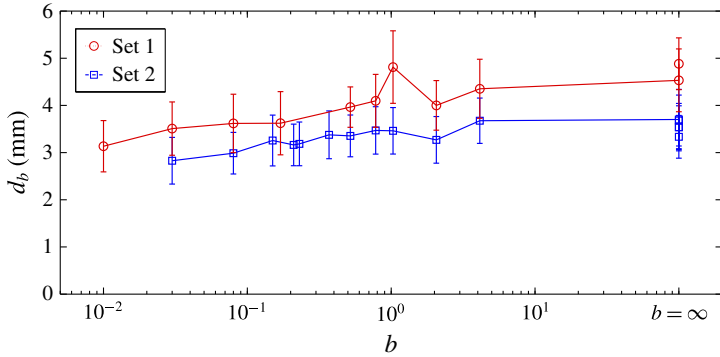in the bubble diameters at higher liquid mean flow speeds is mainly due to the

FIGURE 3. (Colour online) Bubble diameter versus the *b* parameter. The error bars are estimated based on the standard deviations.

fragmentation of the bubbles (as described above) (also see Prakash *et al.* (2012)). Here, the error bars represent the standard deviation of the measured distribution of bubble diameters.

At high mean flow speeds, air is entrained from an open vent at the top of the TWT because of oscillations of the free surface exposed to the atmosphere. The entrained air unavoidably results in microbubbles, which are fed back into the measurement section and contaminate the flow. These entrained microbubbles pose a problem at mean flow speeds higher than 30 cm s^{-1}, and are visible (as very small bubbles) in figure 2(*e,f*). It is necessary to account for these microbubbles in the data analysis, and this issue will be discussed further below.

Also, figure 2(*e,f*) shows instantaneous snapshots of the bubbles at a particular instant of time. Although there might be localised clustering or inhomogeneity of the swarm of bubbles in different regions, these are dynamic and change continuously over time. The homogeneity of the gas phase decreases at low gas volume fractions – this is an inherent limitation in the experiments.

The present experiments in the pseudoturbulence regime ($b = \infty$) for set 1 are essentially the same as the measurements carried out in Martinez Mercado *et al.* (2010), and serve as a reference case for the data analysis and results. For this case of freely rising bubbles in a quiescent liquid, the bubble-based Reynolds number is $Re = d_b U_r / \nu \approx 1000$ (Martinez Mercado *et al.* 2010), where ν is the kinematic viscosity of water (1×10^{-6} m^2 s^{-1}).

2.3. *Phase-sensitive constant-temperature anemometry*

Hot-film anemometry is an important technique in single-phase turbulent flows, but its application in bubbly flows is not straightforward. Since it is an intrusive technique, bubble–probe interactions result in disturbances in the temporal voltage signal from the hot film. Various methods have been developed in the past to remove these 'bubbly spikes' (Zenit, Koch & Sangani 2001; Rensen *et al.* 2005; Martinez Mercado, Palacios Morales & Zenit 2007), so as to exclusively analyse only the liquid fluctuation segments measured by the hot-film probe. For example, a threshold method was used by Zenit (2001) and Martinez Mercado *et al.* (2007) and a pattern-recognition method was used by Rensen *et al.* (2005). These methods essentially come up with an indicator function that labels the gas and liquid phases separately. However, a much better approach to eliminate the bubbly spikes from the CTA signal is to measure the indicator function *in situ* during the experiments.

This can be done by attaching optical fibres with a diameter of $\sim$100 µm close to the hot-film probe (at a distance of $\sim$1 mm) to detect the gas phase. Light is continuously passed through the optical fibre, and when a bubble collides with the probe, the change in refractive index of the gas phase results in a change in signal. This technique, called phase-sensitive constant-temperature anemometry (CTA), was developed by van den Berg *et al.* (2011) and is used in Martinez Mercado *et al.* (2010) and Mendez-Diaz *et al.* (2013). This method can be used to directly detect and remove the bubbly spikes in the hot-film signal.

In this work, we follow almost the same experimental procedure and analysis as in Martinez Mercado *et al.* (2010), but the important difference here is that we vary the *b* parameter over a wide range to cover the regimes between pseudoturbulence ($b = \infty$) and single-phase turbulent flow ($b = 0$). The phase indicator function obtained using information from the optical fibre signal labels the liquid fluctuations and bubble collisions separately. This is used to remove the bubbly spikes and separate the segments containing only liquid fluctuations from the time series signal for further analysis. The power spectrum was calculated for each segment of liquid fluctuation and averaged to obtain the spectrum for a particular case of *b*. The phase-sensitive CTA probe (DANTEC cylindrical probe 55R11) is calibrated by simultaneous measurement of absolute velocities of the single phase using a DANTEC LDA set-up (as in Martinez Mercado *et al.* 2012, Prakash *et al.* 2012). The standard King's law fit is used for the voltage–velocity data. The acquisition rate was 10 kHz and the measurements were carried out for durations of 30 min, and we repeated the experiment once. We average the results from the two experiments for each case of *b*. The CTA–LDA calibration was carried out separately, and once the calibration was done, we did not disturb the probe or experimental set-up and we then took measurements for the different cases of *b*. We kept the duration of experiments short (30 min) to avoid problems with the calibration.

The CTA probe is a fibre-film probe that is suitable for use in liquids; it is more robust than wire probes and less sensitive to contamination. The fibre sensor is a 70 µm diameter quartz fibre, with an overall length of 3 mm, and covered by a nickel thin film approximately 0.1 µm thick. The rated minimum and maximum velocity are 1 and 1000 cm s^{-1}, and the rated maximum frequency limit is 30 kHz. The length of the sensitive area of the hot film is 1.25 mm, and its response time is 0.033 ms. The smallest Kolmogorov time scale of the single-phase turbulence is 35 ms (for a mean flow speed of 65 cm s^{-1}), hence the probe response time is well within the Kolmogorov time scale. Also, the Kolmogorov length scales range from 410 to 200 µm for mean flow speeds ranging between 20 and 60 cm s^{-1} respectively. The sensitive area of the CTA probe (length 1.25 mm) will be able to resolve the Kolmogorov scales. The CTA probe is placed such that the sensitive area is longitudinal or against the flow direction. The optical fibres are attached in such a way that they are antiparallel to the direction of gravity and their tips oppose the rising bubbles. The optical fibres are carefully attached to the CTA probe using permanent glue before the probe is placed in the water tunnel. It has been previously established that the presence of the optical fibres does not compromise the probe's bandwidth and that their infuence on the power spectrum is negligible (van den Berg *et al.* 2011).

The phase-sensitive CTA technique works very well for pseudoturbulent bubbly flows where the bubble diameters are in the range $\sim$2–5 mm. However, when microbubbles collide with the CTA probe, the optical fibres will not be able to register the collision. The reasons for this are twofold: (i) the microbubbles are

small ($\lesssim$300 µm diameter), and (ii) the separation between the CTA probe and the optical fibres is larger ($\sim$1 mm) than the microbubbles. As we mentioned before, microbubbles contaminate the present experiments when the mean flow speeds exceed 30 cm s^{-1}. In these experiments, we inevitably use a threshold method to remove the microbubble collisions, in addition to the phase information obtained from the optical fibres. Further, to keep the data analysis consistent, the combination of the optical fibres and the threshold method is also used in all the experiments except pseudoturbulence, where only the optical fibres are used.

2.4. *Spectrum calculation*

We now consider the spectral distribution of the liquid velocity fluctuations in the different regimes of b. As mentioned in the introduction, the energy spectrum, or, more precisely, the power spectral density (PSD), of the velocity fluctuations has been reported by many authors for both pseudoturbulent and bubbly turbulent flows. The PSD forms therefore a convenient means to describe these flows. We start by explaining how the PSDs were obtained in our case. The PSD was calculated for individual segments of the liquid fluctuations (free from bubbly spikes) using the Welch method (using Hamming windows) at fixed frequencies, and then averaged over all the liquid segments in the measurement to obtain the final result (as in Martinez Mercado *et al.* 2010). The segments selected for the spectrum calculation must have a certain minimum duration to properly resolve all the frequencies; segments that are too short will lack information on the large length scales (low frequencies) and will simply add to the high-frequency components of the spectrum (noise). We investigate the effect of varying this criterion of minimum sample duration (in seconds) on the spectrum for a selected case of $b = 0.23$ (set 2); the results are shown in figure 4. We observe drastic changes in the spectra depending on the value of the minimum sample duration. In figure 4(*a*) we show the spectra directly obtained from the calculation. Both the amplitude and the scaling change, with a monotonic decrease in energy with increasing sample duration. This is expected because when we increase the minimum sample duration considered, we have fewer segments considered and the average energy decreases. In the extreme case of minimum sample duration of 1 s, the spectrum looks noisy because it was averaged over only 80 segments. For the results presented here, we have selected an optimal minimum sample duration of 0.02 s, which nicely resolves all the frequencies (the spectrum is averaged over 14 500 segments). In figure 4(*b*), we show the same spectra after normalising the area under the curve to be equal to unity. We observe that the selected value of 0.02 s is an optimal value; the extreme values (0.002 s, 1 s) show deviations in the scaling. In addition, figure 4(*c*) shows the PDF of the logarithm of the sample durations for three different cases: $b = 0.23, 0.03, \infty$ (set 2). We observe in all cases that more than $\sim$90 % of the samples have a duration longer than our chosen minimum sample duration of 0.02 s; hence our PSD calculations are robust. In the sections that follow, we present results for the normalised spectra in all the cases of b parameter as it allows us to focus solely on changes in the scaling. The energy in the unnormalised spectra depends on the number of samples considered in the averaging, and this can differ in each experiment because it depends on the flow conditions; hence, we normalise the spectra.

3. Results

3.1. *Liquid velocity statistics*

The vertical component of the liquid velocity time series was measured using the phase-sensitive CTA technique at different values of the b parameter. We now consider
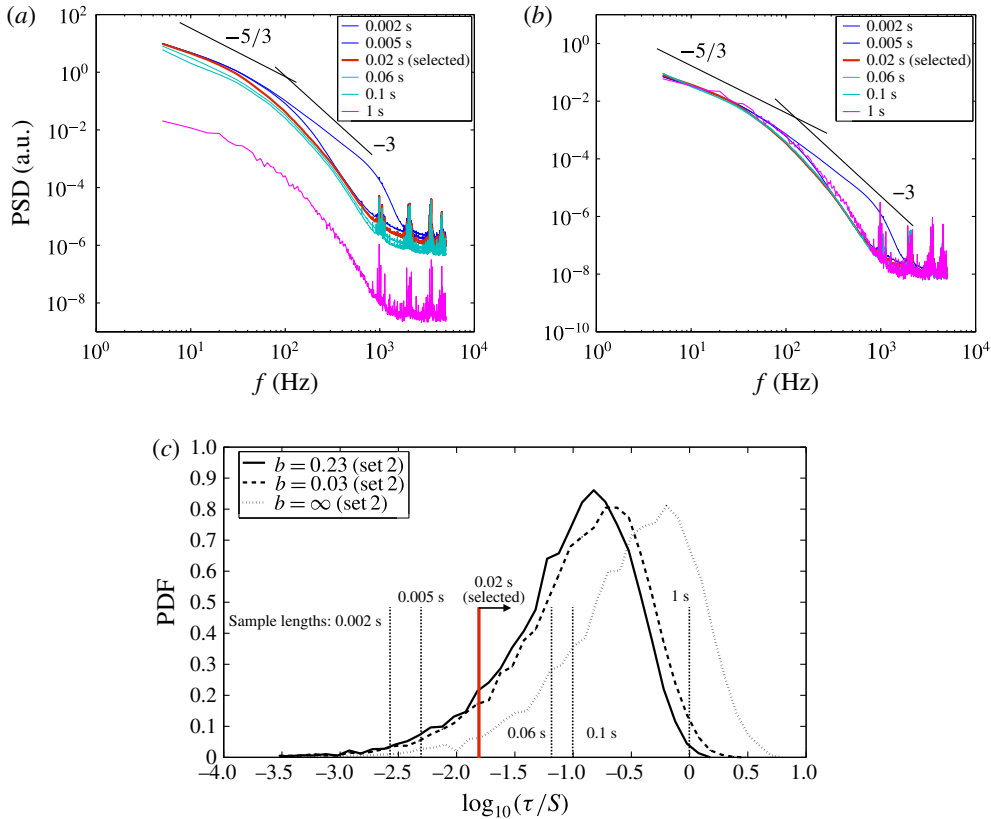
FIGURE 4. (Colour online) Criterion of minimum sample duration for the calculation of the energy spectrum, for the case $b = 0.23$ (set 2): (*a*) unnormalised spectra, (*b*) normalised spectra. The different coloured lines are the spectra obtained with various sample durations, as shown in the legend. The normalised spectrum (*b*) does not change when the sample duration is sufficiently long. A sample duration of 0.02 s is found to be optimal in the present work where the sampling frequency is 10 kHz. (*c*) The PDF of the sample duration used to calculate the spectrum for the cases $b = 0.23, 0.03, \infty$ (set 2). The solid red vertical line corresponds to the selected sample duration of 0.02 s; it is evident (right side of the red line) that more than $\sim 90\,\%$ of the signal is considered for spectrum calculation in all three cases.

the statistics of these fluctuations in liquid velocity using the separated segments of the signal, which are free from bubble collisions. In figure 5, we present the normalised PDFs for the liquid velocity for the different values of b covered in the present work, including experiments in both set 1 and set 2 (see table 1). The PDF of liquid velocity for a single-phase turbulent liquid ($b = 0$) at a mean flow of 30 cm s^{-1} (Taylor Reynolds number $Re_\lambda = 170$) (black dots) nearly follows Gaussian statistics. This single-phase result serves as the reference case.

The liquid velocity PDFs for the cases with bubbles ($b > 0$) are asymmetric and show a deviation from Gaussian behaviour. The positive tails of the PDFs show a higher probability than the Gaussian profile, originating from the flow entrainment in the wake of the rising bubbles, which leads to a larger probability of upward fluctuations (Risso & Ellingsen 2002; Riboux, Risso & Legendre 2010).
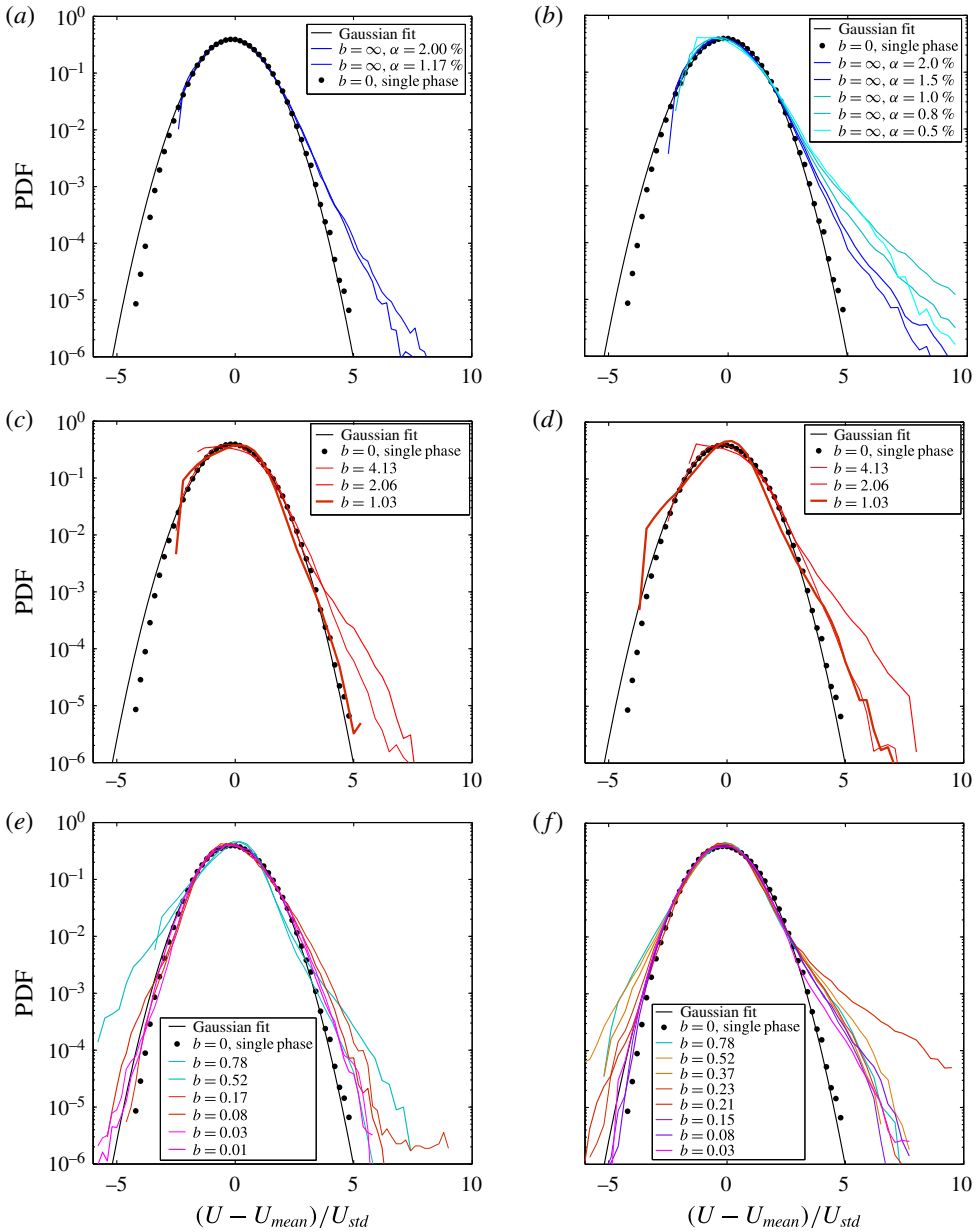
FIGURE 5. (Colour online) PDFs of the liquid velocity normalised by the standard deviation U_{std}, for different b: (a,c,e) set 1, (b,d,f) set 2. (a,b) Represent $b=0$ and $b=\infty$, (c,d) $b=0$ and $b>1$, (e,f) $b=0$ and $b<1$. All the bubbly flow cases show deviations from the Gaussian profile with an enhanced probability of upward fluctuations.

In figure 5 there is no clear trend with respect to the b parameter in the PDFs; the only consistent observation is the asymmetry in the PDFs when bubbles are present ($b>0$). Also, in figure 5, for each row comparing experiments in set 1 and set 2, the PDFs for two similar values of b parameter do not necessarily collapse. Hence, the b parameter does not seem to be a satisfactory single parameter to characterise velocity

statistics in different regimes of turbulent bubbly flow. The positive asymmetry of the PDFs is highest for pseudoturbulence ($b = \infty$), and the asymmetry gradually reduces at smaller b parameter values, probably due to the increase in turbulence levels.

3.2. *Energy spectra*

The PSDs for different values of b are shown in figures 6 and 7. Figure 6(a,c,e) shows PSDs for the experiments in set 1, as given in detail in table 1, and likewise figure 6(b,d,f) for set 2. Frequency is plotted along the horizontal axis in each panel of figure 6. On the vertical axis is the PSD per frequency in arbitrary units but such that the area under the curve in question equals unity. The single-phase Kolmogorov $-5/3$ spectrum, and two lines with slopes $-5/3$ and -3 are shown in all panels of figure 6 as landmarks. Figure 6(a,b) collects all results for the pseudoturbulent case $b = \infty$, but different values of the concentration by volume fraction α. They all clearly follow the k^{-3} line. Figure 6(c,d) shows the results for $b > 1$, whereas figure 6(e,f) shows the results for $0 < b < 1$. From the definition of the bubblance parameter b, measuring the relative importance of the bubbly energy content with respect to the turbulent energy, one may expect dominance of the bubbles for the larger b, say $b > 1$, and therefore spectra of k^{-3} type, and dominance of $k^{-5/3}$ for small values of b ($b < 1$). The first part of this expectation is correct, as figure 6(c,d) shows. The curves for various b values do not exhibit much difference, except that in the higher frequency range, around 100 Hz, there is a slight decrease in energy with increasing b. The second part of the expectation ($k^{-5/3}$ for small values of b), however, is not realised (see figure 6e,f). Surprisingly, even for very small b, the PSD curves have a slope close to -3. Apparently even a small concentration of bubbles alters the PSD significantly and changes it into a PSD much like in the pseudoturbulent case. The same trend is shown in the compensated spectra in figure 7. In figure 7(c,d), it appears that the k^{-3} scaling is followed fairly well.

4. Interpretation of results, discussion and comparison with other work

A better understanding of the results is obtained when we consider a frequency that is representative of the bubbles. Such a frequency is

$$f_b = \frac{U_r}{2\pi d_b}. \tag{4.1}$$

The representative bubble frequencies here are $f_{b1} \sim 9$ Hz and $f_{b2} \sim 12$ Hz when the bubble diameters are in the range $d_{b1} \sim 5\text{–}3$ mm (set 1) and $d_{b2} \sim 4\text{–}2$ mm (set 2) respectively. Since f_{b1} is close to f_{b2}, we consider $f_b \sim 10$ Hz. Now we draw in figure 6(a–f) a vertical line at the value of f_b (~ 10 Hz) pertaining to the two sets of experiments. By doing this we see, as shown in figure 6, an interesting phenomenon: this line marks the transition of the PSD between a part to the left of the line where the $-5/3$ slope is followed and a part to the right where the -3 slope is followed. Energy is fed into the fluid by the bubbles at frequencies close to f_b. This is accompanied by the production of eddies of the size of the bubbles. According to Lance & Bataille (1991), 'the eddies are thus dissipated by viscosity, before spectral transfer can take place'. This explains the separation of the PSD into two parts as described above. Since the eddies do not take part in the large-scale energy transfer, the spectra follow the Kolmogorov $-5/3$ slope in the frequency range between zero and f_b. The energy input by the bubbles passes over
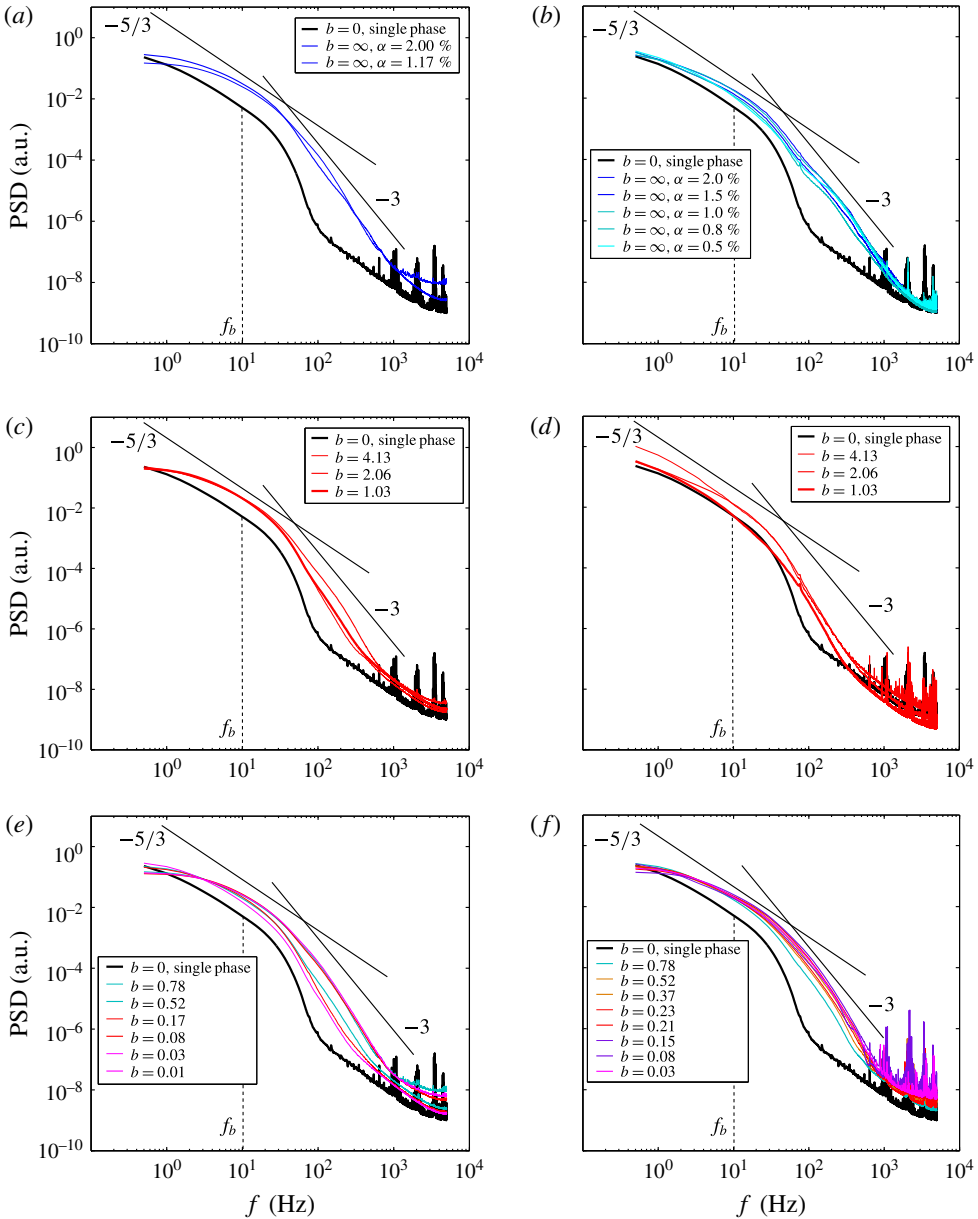
FIGURE 6. (Colour online) The normalised energy spectra at different b: (a,c,e) set 1, (b,d,f) set 2. (a,b) Represent $b = 0$ and $b = \infty$, (c,d) $b = 0$ and $b > 1$, (e,f) $b = 0$ and $b < 1$. All the bubbly flow cases show a deviation from the $-5/3$ Kolmogorov single-phase spectrum beyond the transition frequency (at 10 Hz as indicated by the dotted line), and reasonably follow the -3 scaling.

only to higher wavenumbers. In the steady case, there is an equilibrium between the energy production and the dissipation. In Fourier space the dissipation is $\nu E(k)k^2$, where $E(k)$ is the Fourier transform of the kinetic energy, divided by density, and ν the kinematic viscosity of the fluid. The power input by the bubbles in a uniform
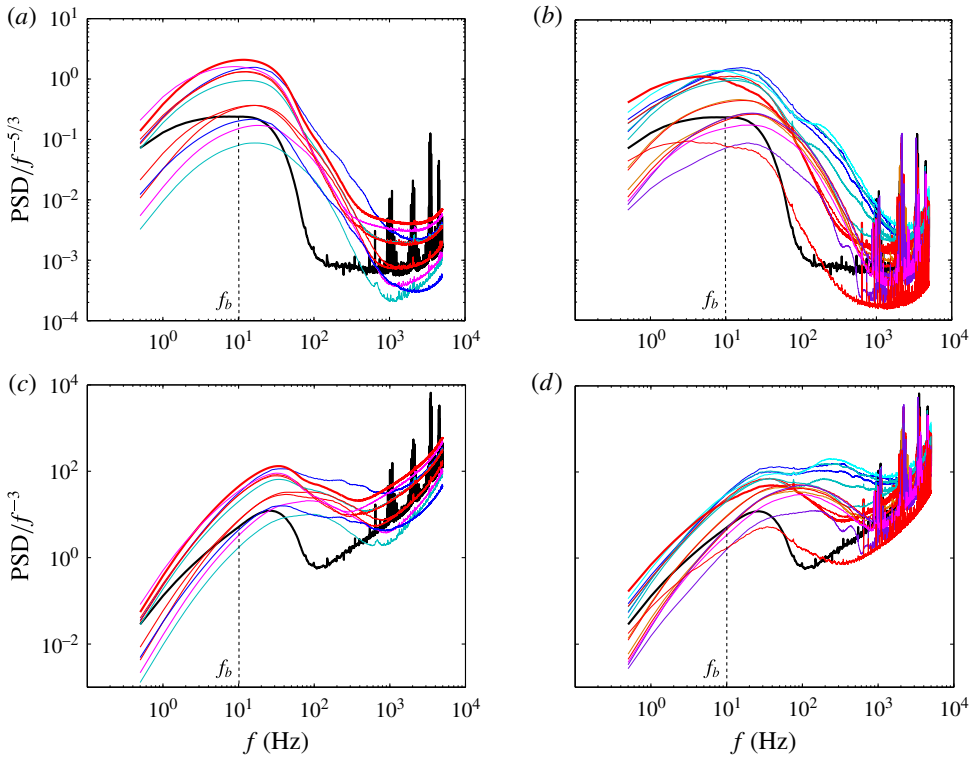
FIGURE 7. (Colour online) The compensated energy spectra at different b: (a,c) set 1, (b,d) set 2. (a,b) Spectra compensated with $-5/3$, (c,d) spectra compensated with -3. The thick black lines indicate the single-phase case. The colours for the bubbly flow cases correspond to the scheme in figure 6. As observed in (c,d), all the bubbly flow cases roughly exhibit the -3 scaling.

bubble distribution is independent of the space coordinate and equal to the work done by buoyancy, which is $\alpha g U_r$ divided by density. Since this is constant, its Fourier transform is $\alpha g U_r/k$, and hence the equilibrium between energy input and energy dissipation in (one-dimensional) Fourier space is

$$\nu E(k) k^2 \sim \frac{\alpha g U_r}{k}. \tag{4.2}$$

This leads to a behaviour $E(k) \sim k^{-3}$, as shown in our experiments. Of course this regime does not go on into the dissipative Kolmogorov scale (η_K). We obtained (4.2) in much the same way as Lance & Bataille (1991) did, with the difference that we used the Fourier transform of the power input.

At the start of our experiments reported in the present paper, we assumed that the bubblance parameter defined in (1.1) would be convenient in marking the transition from $k^{-5/3}$ to k^{-3} behaviour of the spectra. The results indicate that it is rather the bubble frequency, defined in (4.1), that is useful as an indicator of the transition. This, however, opens up the question of the mechanism producing this transition. In particular, the question of how only a few bubbles are sufficient to bring about the k^{-3} spectral scaling behaviour needs to be investigated further. It is clear that

the transition is due to phenomena on the scale of the bubbles. These include the individual bubbles and their wakes, as well as interaction between them. The fluctuations in the experiments by Lance & Bataille (1991) were solely caused by the rising bubbles. Lance & Bataille (1991) made the hypothesis that the k^{-3} behaviour of the spectra is due to the fact that eddies produced by bubbles are dissipated before they can take part in the energy cascade.

The k^{-3} spectrum scaling is a very robust characteristic of pseudoturbulence, as shown in many experimental results, e.g. Riboux *et al.* (2010), Martinez Mercado *et al.* (2010), Mendez-Diaz *et al.* (2013). Here it is shown that also in bubbly turbulent flow this is the case at frequencies above f_b defined in (4.1), independent of the bubble concentration. Also, theoretically the k^{-3} slope in pseudoturbulence has been proven to be robust, because derivations were obtained along different lines. Risso *et al.* (2008) and Risso (2011) distinguished between spatial and time fluctuations of the velocities at a particular point in the bubbly flow, and Risso (2011) found the k^{-3} spectral density for both spatial and temporal parts. Of particular relevance for the present work is the numerical simulation by Riboux *et al.* (2013), in which they considered the flow through a random array of fixed bubbles. Let us say that the mean flow is downward. If we impose an upward velocity on both the fluid and the bubbles, the situation is that of bubbles rising with constant velocity upwards. The bubbles are modelled by sources of fixed momentum distributed randomly, and this flow is very near to what is assumed here in deriving (4.2). Riboux *et al.* (2013) numerically solved the Navier–Stokes equations, and the results for PSDs are shown in their figures 7 and 8 as a function of the reciprocal wavelength λ^{-1}. For the simulations reported in their figures the bubble diameter is 2.5 mm, for which the terminal rise velocity U_r is about 0.3 m s^{-1}. They indeed exhibit the k^{-3} slope in a range between small and large values of λ^{-1}. It is interesting that on the low λ^{-1} side the slope starts to show k^{-3} behaviour at a value of λ^{-1} of about 10^2 m^{-1}. Using $U_r = 2\pi f/k$, one can convert $\lambda_s^{-1} = k_s/2\pi$ into a starting frequency of $f_s \sim 30$ Hz for the -3 scaling. The frequency f_b representative of bubbles of diameter 2.5 mm would, according to (4.1), be $0.3/(2\pi \times 2.5 \times 10^{-3})$ Hz $= 19$ Hz, which is of the same order of magnitude. This indicates that the -3 spectrum scaling first shows up in their simulations also at frequencies higher than the frequency given in (4.1) associated with the bubble size in their simulations. Of course, this correspondence is only qualitative and one should be cautious about attaching further extrapolations to it, bearing in mind as well that in their numerical model there is no external turbulence as in the present study.

5. Summary

In this work, we studied the energy spectra of the velocity fluctuations in different regimes of turbulent flows with varying bubblance parameters (b): single-phase turbulence ($b = 0$), turbulence with some bubbles ($0 < b < \infty$) and pseudoturbulence ($b = \infty$). With varying b, one may expect to find a gradual change in the spectral slope from -3 ($b = \infty$, pseudoturbulence) to $-5/3$ ($b = 0$, single-phase turbulence). However, the results do not show a smooth transition: the -3 spectrum scaling was found at length scales smaller than the size of the bubbles even for very small b values ($b \sim 0.01$), i.e. when the void fraction is as low as 0.1 %. Hence, the bubbles are able to modify the spectra very efficiently, even though they are surrounded by the external turbulent fluctuations. Following the argument by Lance & Bataille (1991), we provided an explanation of the -3 spectrum scaling by balancing the energy

production of the bubbles with the viscous dissipation in Fourier space. The -3 spectrum scaling seems to be a generic feature of turbulent bubbly flows. Regarding the bubblance parameter, in future work, it would be a worthwhile effort to devise a more suitable parameter to characterise turbulent bubbly flows.

Acknowledgements

REFERENCES

VAN DEN BERG, T. H., WORMGOOR, W. D., LUTHER, S. & LOHSE, D. 2011 Phase-sensitive constant temperature anemometry. *Macromol. Mater. Engng* **296**, 230–237.

CLIFT, R., GRACE, J. R. & WEBER, M. E. 1978 *Bubbles, Drops and Particles*. Academic.

CUI, Z. & FAN, L. S. 2004 Turbulence energy distributions in bubbling gas–liquid and gas–liquid–solid flow systems. *Chem. Engng Sci.* **59**, 1755–1766.

DECKWER, B. D. 1992 *Bubble Column Reactors*, 1st edn. Wiley.

ERN, P., RISSO, F., FABRE, D. & MAGNAUDET, J. 2012 Wake-induced oscillatory paths of freely rising or falling bodies. *Annu. Rev. Fluid Mech.* **44**, 97–121.

LANCE, M. & BATAILLE, J. 1991 Turbulence in the liquid phase of a uniform bubbly water–air flow. *J. Fluid Mech.* **222**, 95–118.

MAGNAUDET, J. & EAMES, I. 2000 The motion of high-Reynolds-number bubbles in inhomogeneous flows. *Annu. Rev. Fluid Mech.* **32**, 659–708.

MARTINEZ MERCADO, J., CHEHATA, D., VAN GILS, D. P. M., SUN, C. & LOHSE, D. 2010 On bubble clustering and energy spectra in pseudo-turbulence. *J. Fluid Mech.* **650**, 287–306.

MARTINEZ MERCADO, J., PALACIOS MORALES, C. & ZENIT, R. 2007 Measurements of pseudoturbulence intensity in monodispersed bubbly liquids for $10 < Re < 500$. *Phys. Fluids* **19**, 103302.

MARTINEZ MERCADO, J., PRAKASH, V. N., TAGAWA, Y., SUN, C. & LOHSE, D. 2012 Lagrangian statistics of light particles in turbulence. *Phys. Fluids* **24**, 055106.

MAZZITELLI, I. & LOHSE, D. 2009 Evolution of energy in flow driven by rising bubbles. *Phys. Rev. E* **79**, 066317.

MENDEZ-DIAZ, S., SERRANO-GARCIA, J. C., ZENIT, R. & HERNANDEZ-CORDERO, J. A. 2013 Power spectral distributions of pseudo-turbulent bubbly flows. *Phys. Fluids* **25**, 043303.

MUDDE, R. F., GROEN, J. S. & VAN DER AKKER, H. E. A. 1997 Liquid velocity field in a bubble column: LDA experiments. *Chem. Engng Sci.* **52**, 4217–4224.

POORTE, R. E. G. & BIESHEUVEL, A. 2002 Experiments on the motion of gas bubbles in turbulence generated by an active grid. *J. Fluid Mech.* **461**, 127–154.

POPE, S. B. 2000 *Turbulent Flows*. Cambridge University Press.

PRAKASH, V. N., TAGAWA, Y., CALZAVARINI, E., MARTINEZ MERCADO, J., TOSCHI, F., LOHSE, D. & SUN, C. 2012 How gravity and size affect the acceleration statistics of bubbles in turbulence. *New J. Phys.* **14**, 105017.

RENSEN, J., LUTHER, S. & LOHSE, D. 2005 The effects of bubbles on developed turbulence. *J. Fluid Mech.* **538**, 153–187.

RIBOUX, G., LEGENDRE, D. & RISSO, F. 2013 A model of bubble-induced turbulence based on large-scale wake interactions. *J. Fluid Mech.* **719**, 362–387.

RIBOUX, G., RISSO, F. & LEGENDRE, D. 2010 Experimental characterization of the agitation generated by bubbles rising at high Reynolds number. *J. Fluid Mech.* **643**, 509–539.

RISSO, F. 2011 Theoretical model for k^{-3} spectra in dispersed multiphase flows. *Phys. Fluids* **23**, 011701.

RISSO, F. & ELLINGSEN, K. 2002 Velocity fluctuations in a homogeneous dilute dispersion of high-Reynolds-number rising bubbles. *J. Fluid Mech.* **453**, 395–410.

RISSO, F., ROIG, V., AMOURA, Z., RIBOUX, G. & BILLET, A. M. 2008 Wake attenuation in large Reynolds number dispersed two-phase flows. *Phil. Trans. R. Soc. Lond.* A **366**, 2177–2190.

ROGHAIR, I., MARTÍNEZ MERCADO, J., VAN SINT ANNALAND, M., KUIPERS, J. A. M., SUN, C. & LOHSE, D. 2011 Energy spectra and bubble velocity distributions in pseudo-turbulence: numerical simulations versus experiments. *Intl J. Multiphase Flow* **37**, 1–6.

ZENIT, R., KOCH, D. L. & SANGANI, A. S. 2001 Measurements of the average properties of a suspension of bubbles rising in a vertical channel. *J. Fluid Mech.* **429**, 307–342.